Predominant Interactions between μ-Conotoxin Arg-13 and the Skeletal Muscle Na^+ Channel Localized by Mutant Cycle Analysis†

Nancy S. Chang,‡ Robert J. French,§ Gregory M. Lipkind,|| Harry A. Fozzard,*,⊥ and Samuel Dudley, Jr.⊥,#

Department of Anesthesia and Critical Care, Committee on Clinical Pharmacology, Department of Biochemistry and Molecular Biology, and Departments of Pharmacological & Physiological Sciences and Medicine, The University of Chicago, Chicago, Illinois 60637, and Department of Medical Physiology, University of Calgary, Calgary, Alberta, Canada

Received October 8, 1997; Revised Manuscript Received January 13, 1998

ABSTRACT: High-affinity μ-conotoxin block of skeletal muscle Na^+ channels depends on an arginine at position 13 (Arg-13). To understand both the mechanism of toxin interaction and the general structure of its binding site in the channel mouth, we examined by thermodynamic mutant cycle analysis the interaction between the critical Arg-13 and amino acid residues known to be in the channel's outer vestibule. Arg-13 interacts specifically with domain II Glu-758 with energy of about −3.0 kcal/mol, including both electrostatic and nonelectrostatic components, and with Glu-403 with energy of about −2.0 kcal/mol. Interactions with the other charged residues in the outer vestibule were shown to be almost entirely electrostatic, because these interactions were maintained when Arg-13 was replaced by lysine. These results place the bound Arg-13 at the channel mouth adjacent to the P (pore) loops of domains I and II. Distance estimates based on interaction energies suggest that the charged vestibule residues are in relative positions similar to those of the Lipkind−Fozzard vestibule model [Lipkind, G. M., and Fozzard, H. A. (1994) *Biophys. J. 66*, 1−13]. Kinetic analysis suggests that Arg-13 interactions are partially formed in the ligand−channel transition state.

Important insight into the structure of the outer vestibule of the voltage-gated Na^+ channel has been derived from experimental studies of the effects of point mutations in the channel protein on several channel functions, including guanidinium toxin and Cd^{2+} block, conductance and selectivity, and interaction with cysteine-modifying agents (*2*−*12*). Point mutations have been particularly informative for the binding sites of the marine guanidinium toxins tetrodotoxin (TTX)[1] and saxitoxin (STX) in the channel pore, and this encouraged us to propose a detailed molecular model of the vestibule on the basis of the toxin structures and the residues identified as being important for their binding (*1*). In that proposal, the toxin binding pockets are formed from segments of the S5−6 loops of the four domains. The loops have the secondary structure of β-hairpins, and they are arranged in an antiparallel complex to form a funnel that is complementary to the structures of TTX and STX. The model predicts two rings of mostly charged residues at the top and bottom of the funnel, all of which have been shown experimentally to be critical for guanidinium toxin binding. The inner ring of Asp, Glu, Lys, and Ala residues (DEKA motif) from the P loops of domains I−IV, respectively, is thought to be part of the channel's selectivity filter (*1*, *3*, *8*−*10*). Lipkind and Fozzard (*1*) proposed that the important 1,2,3 guanidinium group of TTX and the 7,8,9 guanidinium group of STX interacted with Asp-400 and Glu-755 residues in the selectivity filter. Glu-403 and Glu-758 of the outer ring of the vestibule are also involved in the TTX site, and additionally, Asp-1532 is involved in STX binding (adult rat skeletal muscle isoform residue numbers).

μ-Conotoxin GIIIA (μ-CTX) is a 22-amino acid peptide produced by the cone snail *Conus geographus* that binds to adult skeletal muscle and eel electroplax Na^+ channels and blocks with nanomolar affinity (*13*−*19*). Its discoidal structure, conferred by disulfide linkage of its six cysteine residues, has been determined by NMR (*20*), and its binding site is known to overlap with the TTX/STX site (*13*). The toxin has a net positive charge (+6 at neutral pH), and blockade by toxin is all-or-nothing with a 1:1 stoichiometry. μ-CTX also shares other characteristics with TTX and STX. A guanidinium group on Arg-13 is critical for high-affinity binding to the channel (*14*, *15*, *18*). Additional observations using the μ-CTX derivative R13Q suggest that Arg-13 is essential for all-or-nothing block of the Na^+ channel (*15*), and interactions with a cytoplasmic pore blocker are con-

† Supported by Grant PO1-HL20592 (H.A.F.), Grant TO1-GM07019 (N.S.C.), the Foundation for Anesthesia Education and Research (N.S.C.), the Medical Research Council of Canada (R.J.F.), and the Alberta Heritage Foundation for Medical Research (R.J.F.).

* To whom correspondence should be addressed.

‡ Department of Anesthesia and Critical Care and Committee on Clinical Pharmacology, The University of Chicago. Present address: Department of Anesthesia, Brigham & Women's Hospital and Harvard University, Boston, MA 02115.

§ University of Calgary.

|| Department of Biochemistry and Molecular Biology, The University of Chicago.

⊥ Departments of Pharmacological & Physiological Sciences and Medicine, The University of Chicago.

Present address: Department of Medicine, Emory University Medical School, Atlanta, GA 30322.

[1] Abbreviations: TTX, tetrodotoxin; STX, saxitoxin; μ-CTX, μ-conotoxin; NMR, nuclear magnetic resonance; HPLC, high-pressure liquid chromatography; IC_{50}, concentration of inhibitor that inhibits 50% of the sodium current.

S0006-2960(97)02492-6 CCC: $15.00
Published on Web 03/11/1998

sistent with the toxin blocking within the pore (*21*). Recently, we demonstrated that Glu-758 is an important channel residue for toxin binding (*19*), and we speculated that the critical guanidinium group of Arg-13 interacts with the channel vestibule in a fashion similar to our proposal where guanidinium groups of TTX and STX interact with the selectivity filter. However, despite these many similarities with TTX and STX, two vestibule residues of importance to TTX and STX binding, Glu-403 and Tyr-401, have been reported to be relatively unimportant for μ-CTX block (*16*, *17*), indicating important differences between the μ-CTX binding site and those of TTX and STX.

In these experiments, we have explored the role of Arg-13 interactions in μ-CTX binding to the skeletal muscle Na^+ channel vestibule by determining the effects of mutations of the several vestibule residues that are known to be important for TTX and STX binding (*2*, *4*−*7*, *11*). The goal was to determine whether Arg-13 does indeed bind within the vestibule and, if so, its interactions. Mutant cycle analysis was used to elucidate the nature of the molecular interactions, because this method allows dissection of the energetic contributions of individual residue pairs in a complex protein−protein interaction. We find that Arg-13 interacts strongly with Glu-758 and less strongly with Glu-403. The interaction with Glu-758 is both electrostatic and nonelectrostatic. Interactions of Arg-13 with other negatively charged residues in the vestibule appear to be entirely electrostatic. The resulting picture of μ-CTX−channel interaction is an insertion of Arg-13 shallowly and eccentrically into the vestibule, closest to the domain II Glu-758 and domain I Glu-403. Block is not achieved by direct interaction with the selectivity filter, and the toxin is more superficial than in the case of TTX and STX. μ-CTX appears to form a partial lid over the vestibule, which under some conditions may allow a narrow path for ion permeation.

MATERIALS AND METHODS

Mutagenesis of μ1. Oligonucleotide-directed point mutations were introduced using the following methods: (1) D400A, E758K, and Y401D with the Unique Site Elimination Mutagenesis Kit (Pharmacia Biotech, Piscataway, NJ) using the methods recommended by the manufacturer; (2) E403Q with the Altered Sites System (Promega, Madison, WI), using the methodology recommended by the manufacturer; (3) E755A with two-primer PCR; (4) K1237A with three-primer PCR (*22*); and (5) D1532N, A1529D, and E758Q with four-primer PCR (*23*). Oligonucleotides containing the desired mutation were designed with changes in silent restriction sites to allow rapid identification of mutants. A vector consisting of the μ1 coding sequence flanked by *Xenopus* globin 5′ and 3′ untranslated regions was provided as a gift by R. Moorman. This was used as the template for mutagenesis, and PCR fragments were isolated and subcloned into this template using directional ligations. Incorporation of mutations was confirmed by DNA sequencing of the entire polymerized regions. The vector was linearized by *Sal*I digestion and transcribed with SP6 DNA-dependent RNA polymerase using reagents from the mCAP RNA Capping Kit (Stratagene, La Jolla, CA). All restriction enzymes were obtained from New England Biolabs, Inc. (Beverly, MA), and all PCR reagents were obtained from Perkin-Elmer (Norwalk, CT).

Synthesis of μ-CTX Derivatives. Reagents were obtained from the following sources: Fmoc amino acids from Novabiochem (LaJolla, CA), Bachem (Torrance, CA), Genzyme (Sygena) (Cambridge, MA), and Richelieu Biotechnologies (Montreal, PQ); Rink amide resin from Novabiochem; HBTU and HOBT from Richelieu; and DIPEA from Aldrich. Organic solvents were obtained from Burdick and Jackson (Muskegon, MI), BDH Inc. (Toronto, ON), and EM Science (Gibstone, NJ).

The linear peptides were synthesized by solid phase synthesis using 9-fluorenylmethoxycarbonyl (Fmoc) chemistry (*24*). Side chain protection was as follows: Cys, trityl; Gln, trityl; Asn, trityl; Arg, Pmc or Pbf; Lys, Boc; Asp, tBu; Hyp, tBu; Thr, tBu; His, trityl; and Glu, tBu. The protected amino acids were used with free carboxylic acid groups. The syntheses were performed on a polystyrene-based Rink amide resin (approximately 0.5 mmol/g), delivering a peptide amide upon cleavage of the linear peptide from the resin. Coupling of the Fmoc amino acids was performed using the HBTU/HOBT/DIPEA method. Single couplings were used for all but the first and the final five, for which double couplings were used. Synthesis was performed on an Applied Biosystems 431A synthesizer.

The raw peptides were air oxidized and purified as previously described (*25*, *26*), with the following modifications. The crude linear peptides were initially desalted on Sephadex G-10/20% acetic acid and then purified by preparative HPLC to ∼90% homogeneity as determined by analytical HPLC. Air oxidation at pH 7.5 was as described by Becker et al. (*25*) except that the volatile buffer, ammonium acetate (50 mM), containing 2-mercaptoethanol (2-ME, 20 μL in 300 mL of solution), was used (peptide concentration was ∼1 mg/mL), and after cyclization, the mixture was acidified with glacial acetic acid before lyophilization (S. Becker, personal communication). Cyclization was monitored by analytical HPLC and was usually complete after 2−3 days at 4 °C. Following folding of the peptide by air oxidation, toxin derivatives were purified to near homogeneity by HPLC (≥95%). Purified peptides were characterized by quantitative amino acid analysis, and in some cases by mass spectroscopy (electrospray) molecular weight determination. Amino acid analyses agreed with theoretical values except for Hyp (∼80−90%) and Cys (∼65−80%). Owing to the limited precision of weighing lyophilized samples, absolute concentrations are accurate to within about ±10%.

As a check that the folded structures did not deviate qualitatively from that of the native toxin, one-dimensional proton NMR spectra were recorded at 15 °C in an aqueous solution containing 5% D_2O at 500 MHZ (D. McIntyre and P. Hwang, personal communication). The proton chemical shifts of the R13X derivatives were generally similar to those of the native toxin, with the exception of the shifts of Asp-12 and Glu-14, for which some change would be expected in response to substitution at the adjacent position 13. Qualitative NOE data indicate that the basic secondary structure remained the same in all cases. Sato et al. (*14*) have also reported that the R13A and R13K derivatives fold normally. The channel-blocking activity of all R13X derivatives was checked by recording from single Na^+ channels incorporated into planar bilayers (K. Hui, I. Sierralta, and R. French, unpublished).

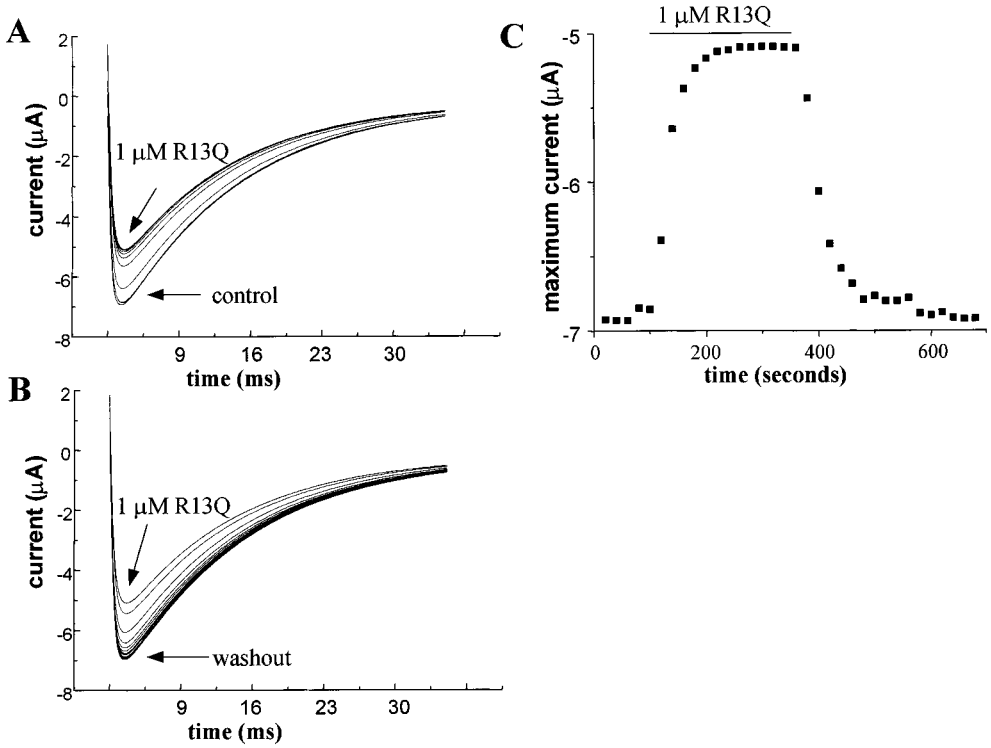

FIGURE 1: Sample current traces showing block of the μ1 Na^+ channel mutant E403Q by the μ-CTX mutant R13Q. Each trace represents the current produced by a voltage step to 0 mV from a holding potential of −100 mV. Voltage steps were administered every 20 s. For this experiment, the IC_{50} was 1.7 μM. (A) Washin of 1 μM R13Q, resulting in a decrease in peak current amplitudes. (B) Washout of toxin with recovery of peak current amplitudes to control levels. (C) Plot of peak currents versus time. The bar indicates the period of exposure to the toxin. Both the development and relief of block were well fit by single-exponential functions. The resulting τ_{on} was 30 s, and the τ_{off} was 51 s, resulting in a K_d of 1.4 μM.

Electrophysiological Recordings. Stage V and VI *Xenopus* oocytes were prepared as previously described in Dudley et al. (*19*). These were injected with approximately 50−100 ng of cRNA using a Drummond microinjector (Broomall, PA). Recordings were made in the two-electrode voltage clamp configuration using a Dagan CA-1 voltage clamp with a series resistance compensation circuit (Dagan, Minneapolis, MN). Electrodes were filled with 3 M KCl and had resistances between 0.3 and 0.8 MΩ. Oocytes were placed in recording chambers in which the bath flow rate was 100 mL/h, and the bath level was adjusted to a total bath volume of ∼250 μL. Data were acquired using pCLAMP6.3 software (Axon Instruments, Foster City, CA) at 71.4 kHz after low-pass filtering at 2 kHz (−3 dB).

The holding potential in all experiments was −100 mV. For K1237A, experiments were also carried out from the holding potential of −120 mV to ensure full availability, and the results were the same at those from −100 mV. Peak currents were measured at 0 mV, with the exception of that for K1237A, for which peak currents were measured at −20 mV. Data were collected from oocytes with peak control currents between 3 and 7 μA, and the measurements of peak currents were made without capacity subtraction. To ensure that this procedure did not bias the results, we performed a comparison of the calculations of IC_{50} and the on and off time constants as described below in a set of 17 experiments with and without capacity subtraction. τ_{on} differed by 3 ± 4%, and τ_{off} differed by 4 ± 2%. IC_{50} differed by 2 ± 3%. These small differences suggested that the capacity correction did not significantly change the results under the conditions of these experiments. Analysis of all recordings, including curve fitting, was performed using the standard equations in pCLAMP6. Peak currents during toxin washin and washout were fit to single exponentials using minimization of the sum of squared errors by the simplex method to obtain first-order rate constants for unbinding and pseudo-first-order rate constants for binding, and used to calculate a kinetic K_d. Further details of this procedure may be found in Dudley et al. (*19*). Return of steady state peak current following washout of toxin was always to within 20% of control levels in each trial, except for the mutant A1529D (see later). In occasional experiments, the development and relief of block were not well-fit by a single exponential, and those experiments were excluded from further analysis. The bath volume was exchanged 5−50 times faster than the fastest time constants, and during preliminary experiments, a doubling of the flow rate did not change the measured time constants. See Figure 1 for an example of currents recorded during the onset and offset of block.

With or without the addition of toxin, recordings were made at room temperature in a standard bathing solution that consisted of (in millimolar) 90 NaCl, 2.5 KCl, 1 $CaCl_2$, 1 $MgCl_2$, and 5 HEPES titrated to pH 7.2 with 1 N NaOH. K1237A was investigated in a solution containing 1 mM $BaCl_2$ instead of $CaCl_2$ to prevent the appearance of calcium-activated outward currents. μ-CTX GIIIA was obtained from either Research Biochemicals International (Natick, MA) or Sigma and stored at −20 °C as a 1 mM stock solution in 1 mM HEPES (pH 7.0). No difference was found in the blocking efficacy of μ-CTX from the two sources.

Because μ-CTX binds to Na^+ channels with 1:1 stoichiometry, and binding results in complete inhibition of ion permeation, the fractional reduction in the peak currents resulting from the application of toxin was taken to represent

the percentage of bound channels. Determinations of IC_{50} were thus made with single concentrations of toxin that were allowed to achieve a steady state of block at holding potential. Achievement of equilibrium was monitored by visual observation of peak currents during brief, depolarizing voltage steps applied at 20 s intervals. The following formula was used to calculate IC_{50} from the average peak currents at equilibrium in the presence of toxin (I_{tox}) and in the absence of toxin (I_{max}):

$$IC_{50} = [\text{toxin}](I_{tox}/I_{max})/(1 - I_{tox}/I_{max})$$

Because the Arg-13 mutants do not completely inhibit ion permeation through single channels, but caused the appearance of fixed subconductance levels when bound, the following modification was used to determine IC_{50} values for these mutants:

$$IC_{50} = [\text{toxin}]X/(1 - X)$$

$$X = (I_{tox}/I_{max} - S)/(1 - S)$$

S is the subconductance level associated with each Arg-13 mutant. Values used for S were 0.56, 0.31, 0.28, and 0.08 for R13D, R13A, R13Q, and R13K, respectively (*27*; K. Hui, I. Sierralta, and R. J. French, unpublished data). Because of the increases in the IC_{50} upon mutation of channel residues, prohibitive amounts of mutated toxins would have been required to assess the residual current levels with each combination of mutant channel and mutant μ-CTX. Therefore, only the residual current levels of μ1 during exposure to saturating concentrations of mutant toxins were determined experimentally, and these agreed well with the single-channel data reported previously. It was assumed that for each channel mutant−Arg-13 mutant pair the residual current was the same as that determined with the comparable native μ1−Arg-13 mutant pair. Residual currents that vary from this assumption would result in errors in the estimations of the IC_{50} values. The kinetically derived K_d would not be affected by this potential source of error, however, and the fact that there was excellent agreement between the K_d and IC_{50} for combinations of mutant toxins with mutant channels (see later) suggested that any differences in the residual currents was not a major source of error.

Because peak current instead of peak conductance was used for kinetic and equilibrium analysis, a shift in the peak current during toxin binding could have resulted in an error in the estimation of the unblocked fraction of channels. Previously, binding of the μ-CTX mutation R13Q to μ1 expressed in tSA-201 cells has been shown to result in as much as a 7 mV hyperpolarizing shift in the I−V relationship (*21*). Under the present experimental conditions, comparison of I−V relationships of μ1 before and during the presence of R13Q showed a similar leftward shift in the peak current (data not shown). When compared at 0 mV, this shift resulted in a less than 10% underestimation of the reduction in peak current associated with binding of R13Q. Since the calculated energy and the coupling coefficient are logarithmically related and since the shift should be similar with mutant and wild-type channels, the overall error in the estimation of coupling energies (see later) would be expected to be quite small. Because of the smaller variance, IC_{50} values were preferred over K_d in the detailed analysis. The residual single-channel currents of R13Q recorded in symmetrical Na^+ solutions were linearly related to voltage over the range of voltages used in this study (G. Zamponi, unpublished observations).

Energy loss due to mutation was calculated as follows:

$$\Delta G = RT \ln[IC_{50}(\text{mutation})/IC_{50}(\text{wild-type})]$$

where R is the gas constant and T is the absolute temperature. Coupling coefficients (Ω) for each mutant toxin−mutant channel pair were calculated as follows (*28*):

$$\Omega = X_1/X_2 = Y_1/Y_2$$

where X_1 = (IC_{50} of mutant toxin−wild-type channel)/(IC_{50} of wild-type toxin−wild-type channel), X_2 = (IC_{50} of mutant toxin−mutant channel)/(IC_{50} of wild-type toxin−mutant channel), Y_1 = (IC_{50} of wild-type toxin−mutant channel)/(IC_{50} of wild-type toxin−wild-type channel), and Y_2 = (IC_{50} of mutant toxin−mutant channel)/(IC_{50} of mutant toxin−wild-type channel). Transformation of Ω into coupling energy ($\Delta\Delta G$) was calculated as $RT \ln \Omega$.

Molecular modeling was performed with Biosym software (Biosym Technologies, Inc., San Diego, CA) operating on a Silicon Graphics Elan 4000 workstation, as described by Dudley et al. (*19*). All energy calculations were based on the Biosym consistent valence force field (cvff), wherein electrostatic interactions and hydrogen bonds are calculated as Coulombic energies between charges or partial charges. The dielectric constant was assumed to be 31 (*19*). Structural optimization was performed by minimizing the potential energy surface predicted by the cvff using iteration of steepest descents or conjugate gradients. van der Waals (nonbonded) energies were based on the Lennard-Jones 6,12 potential.

RESULTS

Characteristics of the μ1 Mutants. Na^+ currents in the microampere range were expressed for all of the following mutants: D400A, Y401D, and E403Q from domain I; E755A, E758Q, and E758K from domain II; K1237A from domain III; and A1529D and D1532N from domain IV. The mutants showed Na^+ currents with voltage- and time-dependent properties similar to those of the wild-type currents (data not shown), implying that the structural and functional features of the channels remained intact. As expected, K1237A showed a change in the reversal potential to 2.6 ± 5.9 mV (compared to the reversal potential of the wild-type channel of 45.5 ± 2.8 mV), and smaller changes were also seen in E755A and A1529D (33.7 ± 0.7 and 34.8 ± 4.2 mV), consistent with their location in or near the selective filter (*3*, *9*, *10*, *29*).

Effects of μ1 Mutants on μ-CTX Block. The mutations at Glu-758 had the greatest effect on the IC_{50} measurements of μ-CTX block: 76-fold for E758Q and 762-fold for E758K (Table 1A and Figure 2). More modest effects were seen with the other pore residue mutants. Y401D and D1532N each caused an approximately 15-fold decrease in blocking efficacy. E755A produced an 11-fold reduction, and D400A and E403Q produced an approximately 8-fold reduction. The mutant A1529D exhibited very slow kinetics for development and relief of block, and recovery of currents was rarely more

Table 1: Effects of μ1 and CTX Mutants on Toxin Binding

(A) Effects of μ1 Mutants

μ1 mutant	k_{on} (M^{-1} s^{-1})	SE	k_{off} (s^{-1})	SE	K_d (nM)	SE	IC_{50} (nM)	SE	IC_{50} ratio[a]
μ1	2.1×10^5	4.2×10^4	1.9×10^{-3}	1.2×10^{-4}	10.8	3.1	11.7	2.8	1.0
D400A	9.7×10^4	2.3×10^4	6.6×10^{-3}	8.4×10^{-4}	90.2	19.5	97.7	16.2	8.3
Y401A	1.1×10^5	2.7×10^3	1.1×10^{-2}	1.5×10^{-3}	95.5	12.2	180.8	8.4	15.4
E403Q	1.4×10^5	3.0×10^4	1.6×10^{-2}	1.5×10^{-3}	130.0	17.0	98.0	9.1	8.3
E755A	8.1×10^4	2.3×10^4	7.0×10^{-3}	7.3×10^{-4}	144.9	46.5	133.4	19.4	11.4
E758Q	1.0×10^4	3.1×10^3	8.3×10^{-3}	9.6×10^{-4}	1393.1	320.9	896.7	98.3	76.3
E758K	3.0×10^3	1.4×10^3	7.4×10^{-3}	1.1×10^{-3}	6788.0	2703.8	8949.4	2165.4	761.8
K1237A	9.5×10^4	1.6×10^4	4.1×10^{-3}	4.2×10^{-4}	56.6	17.1	41.8	10.9	3.6
D1532N	3.7×10^4	1.3×10^4	7.9×10^{-3}	8.3×10^{-4}	360.3	79.5	164.4	22.7	14.0

(B) Effects of CTX Mutants

CTX mutant	k_{on} (M^{-1} s^{-1})	SE	k_{off} (s^{-1})	SE	K_d (nM)	SE	IC_{50} (nM)	SE	IC_{50} ratio[a]
μ-CTX	2.1×10^5	4.2×10^4	1.9×10^{-3}	1.2×10^{-4}	10.8	3.1	11.7	2.8	1.0
R13K	3.1×10^4	5.9×10^3	6.5×10^{-3}	1.1×10^{-3}	232.9	41.0	196.3	28.1	16.7
R13Q	6.1×10^3	2.6×10^3	1.7×10^{-2}	3.2×10^{-3}	4326.6	916.0	1412.1	146.8	120.2
R13A	5.2×10^3	1.1×10^3	1.1×10^{-2}	9.4×10^{-4}	2807.7	1059.4	2452.5	746.2	208.8
R13D	3.7×10^3	1.4×10^3	2.1×10^{-2}	9.8×10^{-3}	5310.7	599.2	8933.3	1080.9	760.4

[a] The IC_{50} ratio is the ratio of mutant to wild-type IC_{50}.

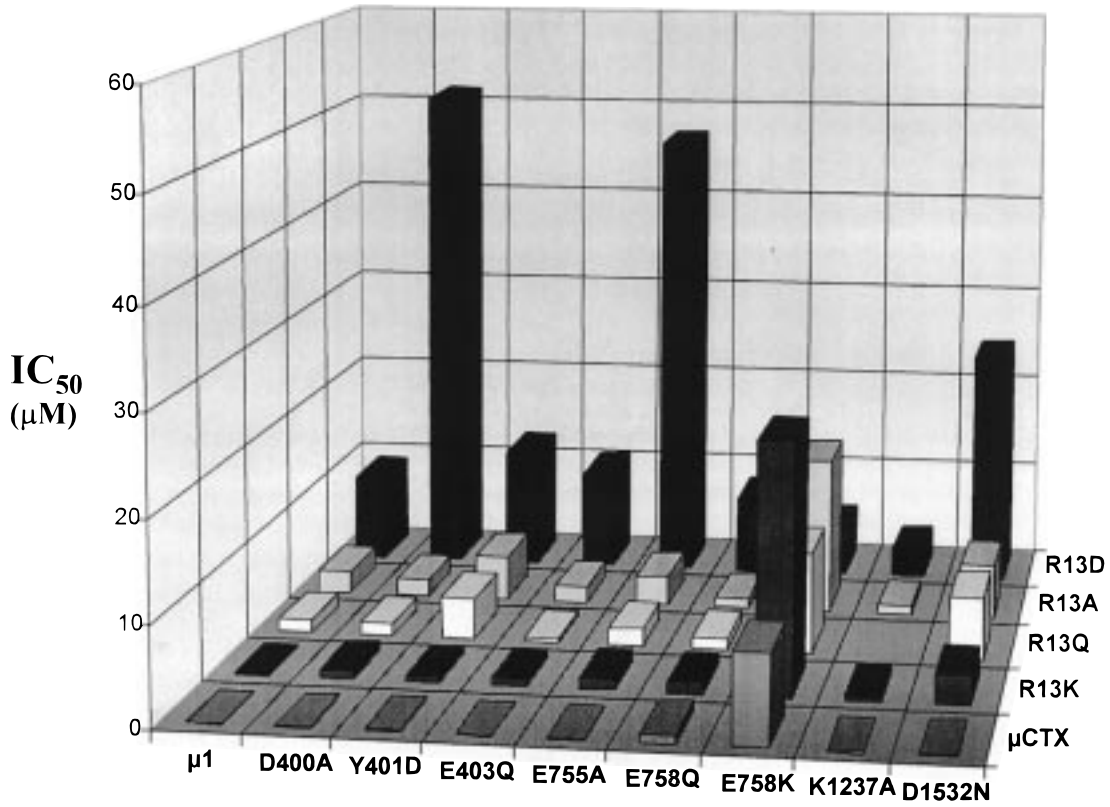

FIGURE 2: Equilibrium blocking affinities (IC_{50}s) for the channel−toxin pairs. Affinities tended to decrease progressively as μ-CTX Arg-13 was mutated to the charge-conserving lysine, then to charge-neutralizing glutamine and alanine, and then to charge-reversing aspartate. One significant exception to this pattern is E758K, where reversal of the charges led to an improved binding affinity. Standard errors reported in Table 1 are representative of this data set, so error bars are omitted for clarity. For all measurements, $n \geq 3$. Full data sets are available on request.

than 50−60%. This prevented accurate measurement of the equilibrium IC_{50} with this mutant; however, the wild-type μ-CTX appeared to bind to the mutant A1529D with an affinity similar to that of the wild-type channel (13 nM). Because of the slow kinetics, A1529D was not studied further.

The effects of channel mutants on the kinetically determined K_d were similar to those on the IC_{50} measurements (Table 1A). Because several sources of error in the affinity measurements differ between these two parameters, the agreement between these different methods of estimating affinity provides evidence that the possible measurement errors in IC_{50} and K_d are not large. All channel mutants affected k_{off}. (Figure 3A and Table 1A). The largest k_{off} effect was seen with the mutant E403Q (9-fold); other changes were less than 5-fold. Mutation of two of the outer ring residues showed significant effects on k_{on}, with the largest effects for the Glu-758 mutants. Overall, kinetic effects were seen with all charged channel mutants and were largest for mutations of Glu-758.

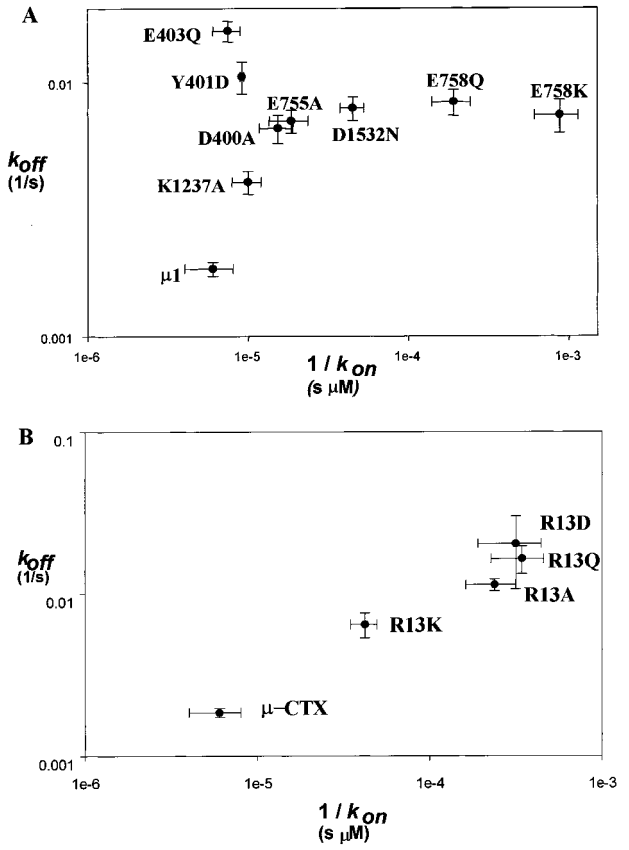

FIGURE 3: Relation between k_{on} and k_{off}. Dissociation rate constants and their standard errors are plotted against the reciprocal association rate constants for μ1 mutants (A) and μ-CTX Arg-13 mutants (B). Channel mutants mainly affected dissociation rates, except for Asp-1532 and Glu-758, which also had significant changes in association rates. Toxin mutants affected both rate constants. Points nearest to the lower left-hand corner of each plot represent the highest binding affinities.

Effects of Arg-13 Mutations. Becker et al. (*15*) and Dudley et al. (*19*) previously suggested that the toxin residue Arg-13 interacts directly with the channel pore to produce block. In these experiments, mutations of Arg-13 certainly had dramatic effects on μ-CTX block of the Na^+ current (Table 1B and Figure 2). The calculation of mutation-induced changes in IC_{50} is complicated by incomplete block by some Arg-13 mutations (see Materials and Methods). The charge-conserving mutation with Arg replaced by Lys (R13K) reduced blocking efficacy 17-fold, calculated on the basis of an estimated 8% residual current (see ref *27* for discussion of this value). Neutralization by replacement with glutamine (R13Q) caused a further 7-fold decrease in IC_{50}, based on a 28% residual block (120-fold, relative to the native toxin). A similar blocking efficacy was seen with R13A (209-fold). Reversal of charge with glutamate (R13D) produced an additional 5-fold reduction in affinity, using the estimated residual current figure of 56%. The reduction was 760-fold compared to the IC_{50} of the unmutated μ-CTX. The kinetically determined K_d values agreed well with the IC_{50} values, supporting the validity of the corrections in IC_{50} from estimates of residual currents. Both k_{on} and k_{off} changes were seen with Arg-13 mutations (Figure 3B and Table 1B).

Double Mutant Cycle Analysis. Interpretation of the role of a mutated residue in protein−protein interaction simply by loss of interaction energy can be misleading. For example, it is likely that Arg-13 interacts with multiple channel residues, and channel residues may interact with toxin residues other than Arg-13. A more discriminating approach is mutant thermodynamic cycle analysis. In its simplest form, exclusive interaction between two residues can be equally disrupted by mutations of either of the pair. If one is mutated, then mutation of the other should be without effect. On the other hand, if the two mutations produce independent effects, then the two mutations should have a simple additive effect. Systematic analysis of the extent of coupling between two residues has been developed by Fersht and colleagues (*30*−*33*). For example, Schreiber and Fersht (*34*) examined the roles of interactions between pairs of residues in the enzyme−inhibitor complex of barnase and barstar, for which the crystal structure is known. The thermodynamic cycle analysis method was first applied to a toxin interaction with a channel by Hidalgo and MacKinnon (*28*). For this analysis, four interactions are measured: wild-type channel with wild-type toxin, mutant channel with wild-type toxin, mutant toxin with wild-type channel, and mutant channel with mutant toxin. A coupling coefficient Ω is calculated, which is a function of the energy of interaction between the two residues. Although Schreiber and Fersht (*34*) estimated the error in this variable to be about 0.5 kcal/mol under their experimental conditions, we have considered interactions in these experiments to be significant if mutations showed a 1 kcal/mol change ($\Omega \geq 5$), to minimize any nonspecific effects under our experimental conditions.

The coupling coefficients were much larger for the Arg-13−Glu-758 mutations than for any others (Figure 4), supporting the interpretation that Arg-13 interacts primarily with Glu-758. The smallest mutational effects were seen for the charge-preserving mutation R13K. The R13K mutation did not produce significant Ω values ($\Delta\Delta G < 1$ kcal/mol) with any of the vestibule residue mutants tested except Glu-758. The simplest explanation for this is that the interaction of Arg-13 with these other residues was not much altered when the charge is conserved. Significant values of Ω were obtained with R13Q, -A, and -D for interactions with D400, Y401, E403, E755, K1237, and D1532. In addition, the domain III P loop contains a charged residue, Asp-1241, which when neutralized reduces μ-CTX affinity (*35*). Asp-1241 is usually considered to be outside the vestibule, and it has only a modest effect on TTX and STX affinity (*2*, *7*). No interaction was found between Asp-1241 and Arg-13 ($\Omega = 2$; N. S. Chang, unpublished observations).

Reversal of Charges at Glu-758 and Arg-13 Partially Recapitulates Wild-Type Block. With the channel mutations studied, the greatest decrease in blocking efficacy for μ-CTX was seen with the charge-switching mutant E758K (762-fold) (Figure 5). Similarly, among the R13 mutants, the charge-switching mutant R13D reduced block the most (760-fold). Exposure of the mutant channel E758K to the mutant toxin R13D showed a modest improvement in block, only 425-fold less than those of wild-type channel and toxin. Because the R13D/E758K pair cannot be expected to recover the arginine-specific energy of interaction, the R13K mutant may more closely represent the control for a pure electrostatic interaction between two oppositely charged residues at this site, without restoration of nonelectrostatic forces. This difference is only 25-fold (Figure 2). The improvement in binding by restoration of the charge pair is highly suggestive

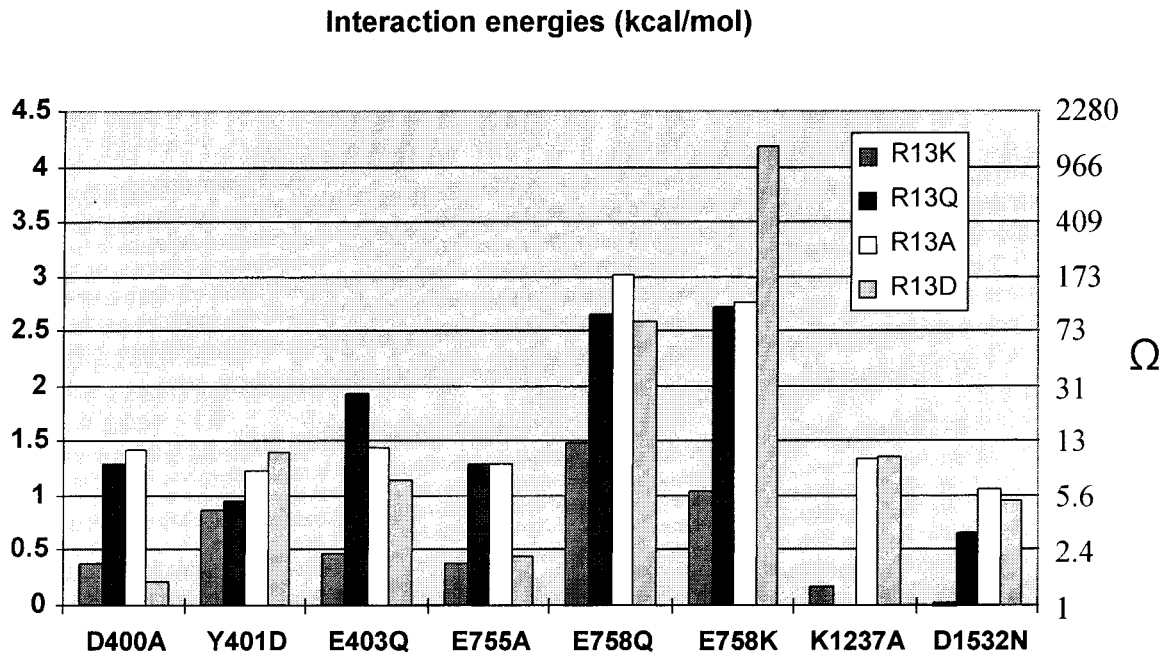

FIGURE 4: Interaction energies. Calculated interaction energies ($\Delta\Delta G$) for the mutant pairs in kilocalories per mole. Corresponding Ω values are shown on the axis to the right.

of a close electrostatic interaction between Arg-13 and Glu-758 during toxin binding, but emphasizes that other interactions are important for the Arg-13−Glu-758 complex. Complete restoration of binding energy could not be expected because the negative charge of R13D would still interact unfavorably with the field produced by the other negative pore residues. This further supports the conclusion that the Arg-13 mutants are arranged in the outer vestibule in a manner similar to the arrangement for native μ-CTX.

DISCUSSION

Arg-13 is known to be the toxin residue that is most important for μ-CTX binding (*14*, *15*, *18*). Therefore, we tested the hypothesis that Arg-13 of μ-CTX interacted with the outer vestibule of the Na^+ channel in a manner similar to that of the guanidinium groups of STX and TTX (*1*, *19*). Thermodynamic mutant cycle analysis was used to isolate and quantify the individual interactions of Arg-13 with key amino acids in the vestibule that are known to interact with TTX and STX. Our results confirm that this residue is very important for μ-CTX binding affinity. μ-CTX binds to the Na^+ channel outer vestibule, and Arg-13 accounts for most of the energy of interaction between the toxin and the charged residues in the outer vestibule. Arg-13 interacted most strongly with the vestibule's outer charged ring, and given the shape of the toxin, this suggests that the remaining residues of the P loops of the channel form a shelf outside the vestibule, preventing μ-CTX from entering more deeply into the pore. Some Arg-13 interactions form early in the μ-CTX−channel complex, according to kinetic analysis, and others form late.

Arg-13 Controls μ-CTX Affinity. The effects of various Arg-13 mutations on blocking affinity and kinetics were assessed. No Arg-13 mutation improved blocking affinity compared with that of the native μ-CTX. There was a trend toward worsening the blocking efficacy as Arg-13 substitutions progressed from R13K to R13Q to R13A to R13D (Figures 2 and 4). This trend argues that the orientation of the toxin with respect to the channel is not changed by the Arg-13 mutations, a possibility that had been suggested recently by Chahine et al. (*18*). This trend could be explained on the basis of the type and extent of interactions lost when Arg-13 is mutated to the other amino acids. A plausible description of the underlying mechanisms of the trend is as follows. The transition from the native arginine to lysine would be expected to preserve most of the electrostatic component of the interaction, but with the loss of any arginine-specific binding component. The glutamine substitution has the potential for maintaining hydrogen bonds but is not capable of recapitulating the electrostatic component of the original toxin. Alanine substitutions should have eliminated all significant interactions between the toxin site 13 and the channel. Finally, the aspartate substitution introduces a new electrostatic repulsive force.

The implications of these results are that Arg-13 has a unique interaction with the channel that consists of both electrostatic and nonelectrostatic components. The majority of the Arg-13 interaction with the native channel is specific to arginine. Mutation of Arg-13 to lysine caused an association energy loss of 1.6 kcal/mol based upon the ratio of the IC_{50} values for Arg-13 and R13K. The mutation R13A resulted in a total loss of 3.1 kcal/mol, which would be expected to represent the total energy in the Arg-13−channel interaction. Therefore, the R13K mutation accounted for more than half of the energy lost. The second largest loss of association energy with the native channel occurred when lysine was exchanged for glutamine. The energy loss was 1.2 kcal/mol, providing a lower limit on the electrostatic component to the Arg-13−channel interaction. Finally, a small additional loss of energy was seen when alanine was substituted for glutamine, suggesting that glutamine may have maintained some interactions with the channel, possibly through hydrogen bonding. Substitution of the negatively charged aspartate for alanine resulted in a 0.8 kcal/mol

repulsive energy that suggested that Arg-13 is normally proximate to channel carboxyl groups and within the negative field of the vestibule.

The kinetic measurements support the idea that Arg-13 does not act solely as an electrostatic attractor of the toxin for the channel. A statistically significant change in k_{on} when mutating Arg-13 to lysine ($p = 0.02$) demonstrated that k_{on} was not exclusively determined by electrostatic considerations (Figure 3B). A comparison of the native μ-CTX with R13K, R13Q, R13A, and R13D demonstrated that k_{on} decreased 7-, 34-, 40-, and 56-fold, respectively. The change seen with R13K represents some form of advantage arginine has over lysine in the activated state. Furthermore, pure electrostatic attractors are generally thought to affect exclusively the ligand on rates (*36*). In these experiments, there was a statistically significant correlation coefficient ($r = -0.78$, $p < 0.2-0.1$) between the changes in k_{on} and k_{off} resulting from an Arg-13 mutation. The changes in k_{on} were larger than those of k_{off}, but plotting the logarithm of the ratio of the Arg-13 mutant kinetic rates to that of the native toxin (the relative change in the activation energy) as a function of the change in charge showed that k_{on} did not have a linear relationship with the change in charge at the Arg-13 site. Interestingly, the relationship was more linear for k_{off} than for k_{on}, contrary to the prediction of Escobar et al. (*36*).

μ-CTX Binds to the Outer Vestibule. All channel mutations worsened the native μ-CTX affinity, with the possible exception of A1529D. As assessed by the change in IC_{50} by mutagenesis (ΔG), the loss of energy associated with channel mutations was in a relatively narrow range of 1.2−1.6 kcal/mol except for the E758Q and/or -K (2.5 and 3.9 kcal/mol) and K1237A (0.7 kcal/mol) mutations. The rank order of importance of channel residue substitutions on the IC_{50} was E758K > E758Q > Y401D ≈ D1532N ≈ E755A ≈ E403Q ≈ D400A > K1237A.

The relative importance of the residues contributed by each channel domain and the relative effects of residues within a vestibule ring suggested that μ-CTX has a stronger and more specific interaction with the outer ring. The IC_{50} changes were smaller for D400A and E755A and were indistinguishable ($p = 0.18$), suggesting that these residues were having equivalent effects on μ-CTX binding. Furthermore, these mutations of the inner ring had a statistically indistinguishable effect on k_{on} and k_{off} ($p = 0.26$). Note that, in contrast, Asp-400 or Glu-755 mutations have a profound effect on TTX and STX binding (*2*). In the outer ring, domain II was most important for μ-CTX, followed by domain I and then by domain IV, a pattern consistent with a specific close-range interaction with domain II.

As with mutations of Arg-13, channel mutations did not appear to affect μ-CTX affinity solely through changes in electrostatic attraction, supporting the presence of close interactions between μ-CTX and the outer vestibule. Changes in energy resulting from mutations at Glu-758 were not a linear function of the change in charge, emphasizing the contribution of nonelectrostatic components. On electrostatic considerations, both Y401D and K1237A should have increased μ-CTX binding because of the increase in the net negative potential of the vestibule, but both mutations resulted in a loss of affinity. Because both k_{on} and k_{off} were affected, the effect of channel mutations on kinetics also was not indicative of alterations in pure electrostatic interactions and suggested a close interaction between μ-CTX and the outer vestibule.

The effects of the channel mutations on the kinetics of toxin interaction appeared to fall in two groups. Mutations of outer ring residues Asp-1532 and Glu-758 resulted in a fixed reduction in k_{off} ($p = 0.81$), and the differences between their IC_{50} values were brought about by changes in k_{on}. Kinetic analysis showed a trend toward a reduction in k_{on} and a significant acceleration of k_{off} of native μ-CTX for Glu-758 mutants as compared with native channels (Figure 3A). This could be the result of a link between the energies of the activated and the final bound states giving constant k_{off} values and varying k_{on} values. The remainder of the mutations appeared to have their effects on the IC_{50} mostly through changes in k_{off}, and the energy of the activated state appeared to be independent of the energy of the final bound state, suggesting that these residues were most important for stabilizing the final, bound state. Effects of all outer vestibule mutants on k_{off} suggested close-range interactions of the outer vestibule with some portion of μ-CTX in the final, bound state.

Arg-13 Is the Principal Residue Interacting with the Outer Vestibule. Because our ultimate goal is to use μ-CTX as a molecular caliper for the structure of the outer vestibule, assignment of the energy change resulting from mutagenesis of the toxin or channel to a particular interacting pair is desirable. Effects of μ-CTX or channel mutations on the IC_{50} values are not generally the result of loss of one specific, individual interaction between a pair of residues on the channel and toxin, respectively. For example, a single carboxyl group in the outer vestibule might be expected to attract several positive charges on μ-CTX, and neutralization of R13 would have a larger effect on the IC_{50} values than the elimination of any single toxin−channel interacting pair. Thermodynamic mutant cycle analysis is helpful in assigning interactions to specific residue pairs.

Arg-13 showed significant coupling with each outer vestibule residue that is involved in TTX and STX interaction, but the level of interaction with Glu-758 was much greater than the others. These results confirm our previous predictions about Glu-758 interactions (*19*) and support the idea that Arg-13 interacts with the outer vestibule to inhibit current. Furthermore, the interaction observed at the Tyr-401 site is consistent with the experimental results of Chahine et al. (*18*).

Calculation of the coupling coefficient Ω assumes that the pair of mutations eliminates a specific interaction between them so that Ω represents the total energy of the interaction (*37*). The dependence of Ω on the group substituted in the Arg-13 position was used to probe the nature of interactions between Arg-13 and particular groups on the channel (*38*) (Figure 4). As noted previously for Arg-13 mutations and the native μ1 channel, IC_{50} values tended to increase progressively in the charge-neutralizing mutant channels when Arg-13 was substituted for lysine, then glutamine, and alanine, presumably representing a progressive loss of arginine-specific interactions, electrostatic interactions, and hydrogen bonding. This suggestion is supported by the increasing number of significant Ωs for the channel mutants when varying the Arg-13 substitution from lysine to glutamine and then to alanine. As already noted, the fact that Ω varied

in this way suggested that mutations of the channel or the toxin did not result in major structural changes in either entity or in the toxin binding orientation.

All interacting pairs except for those involving Glu-758 had a predominately electrostatic interaction, and the inner ring had an exclusively electrostatic interaction. Channel residues with a large electrostatic component of the interaction with Arg-13 would be expected to have an Ω of >5 for R13A and an Ω of <5 for R13K. In addition, residues with exclusively electrostatic interactions would be expected to show R13Q Ωs similar to those of R13A. Therefore, it appeared as if inner ring residues Asp-400 and Glu-755 had only electrostatic interactions with Arg-13.

On the other hand, Arg-13 appeared to have a specific interaction with Glu-758 of the outer ring involving components in addition to electrostatic forces. On the basis of the Ω values, the interaction between Arg-13 and Glu-758 was much stronger than those with other outer vestibule sites. This interaction appeared to consist of arginine-specific electrostatic, and hydrogen bond components as suggested by the change in Ω with various Arg-13 substitutions (Figure 4). The extraordinarily large Ω with the combination of E758K/R13D confirmed that there was a close interaction of these residues and that neither the structures of the channel nor μ-CTX had been significantly altered by the mutagenesis.

Arg-13 also seems to have a smaller but significant interaction with Glu-403. The total E403Q/R13Q interaction energy change ($\Delta\Delta G$) was almost 2 kcal/mol, most of which appeared to be electrostatic. This is somewhat more than expected from the results of Stephan et al. (*17*), who reported a ΔG of 0.8 kcal/mol for binding of μ-CTX GIIIA by the E403Q mutant. Li et al. (*39*) reported no change in blocking affinity with the mutation E403C. Neither of those investigations employed mutant cycle analysis, which avoids some of the sources of error in mutational studies. Similar to the differences between ΔG and $\Delta\Delta G$ seen in our experiments for E758Q, there may have been partial compensation for the loss of Glu-403. In any case, Glu-403 appeared to have the next most important interaction with Arg-13 after Glu-758.

The Arg-13 residue plays a large role in the binding of μ-CTX, and much of the outer vestibule−Arg-13 interaction is accounted for by the interaction of Arg-13 with Glu-758. On the basis of the ratio of the IC_{50} for the native channel, the loss of energy when Arg-13 was replaced by alanine was 3.1 kcal/mol. The total E758Q/R13A interaction energy change was 3.0 kcal/mol. Therefore, it is likely that the binding energy loss associated with Glu-758 neutralization was explained by the loss of the Arg-13−Glu-758 interaction, and much of the Arg-13 total interaction energy with the channel was also in this association. It is interesting that the single mutation E758Q resulted in only a 1.2 kcal/mol energy loss, as if Arg-13 can partially compensate for loss of Glu-758.

Limitations to the Calculation of Energy Changes. The correlation between the sum of the ΔGs caused by channel mutations and the $\Delta\Delta G$ calculated from the Ω values suggested that all of the energetically important Arg-13 interactions with the channel were identified. In general, the $\Delta\Delta G$ for interaction with Arg-13 should have been less than or equal to the ΔG for any channel mutation, and the sum of the energies of interaction between Arg-13 and groups on the channel based on the Ω should approximate the total energy lost when mutating Arg-13 to alanine which was calculated by the ratio of the IC_{50}. Comparison of ΔG values for a channel mutation with $\Delta\Delta G$ values for R13A showed that $\Delta\Delta G$ was greater than the ΔG for E758Q and K1237A, approximately equal for E403Q, D400A, and E755A, and less than that for D1532N, Y401D, and E758K. Quantitative errors in the $\Delta\Delta G$s include failure to take into account energies of hydration, changes in counterion concentrations, movement of residues, or a strain in the proteins brought about by various mutations. Also, it seems likely that there would be compensatory movement of side chains of both Arg-13 and other charged residues when there is a change in the net charge.

One source of error in the energies calculated from Ω could have been the introduction of new, unanticipated forces with the mutant combination. In mutant cycle analysis, all deviations from the predicted IC_{50} for the combination of mutations are ascribed to a loss of energy of interaction. This may not be the case, and furthermore, new forces may be introduced. For example, R13D−channel mutant pairs sometimes showed lower Ω values than their respective R13A pairs (Figure 4). New repulsive forces introduced between the channel and R13D might explain this phenomenon. A similar repulsive force between R13K and E758K probably explains why this Ω is smaller than might be expected. The lack of difference between the E758K/R13Q and E758K/R13A Ω values supports this assertion. However, movement of the lysines in the R13K and E758K mutations relative to the positions of the native arginine and glutamates cannot be ruled out as a contributory factor in the lower Ω. Supporting evidence for the introduction of unanticipated forces with mutations includes the opposing directions of the IC_{50} changes seen by comparing the native channel and channel mutants. Several mutant combinations showed an improved affinity compared with the same R13X−μ1 combination. This can be explained by introduction of new, unanticipated forces in the R13X−channel residue pair, since the IC_{50} ratio should have been close to 1.0.

Kinetic Measurements and Transition States. Assuming a constant pathway of interaction between μ-CTX and the channel and no intermediate states with less free energy than the initial solution states of μ-CTX, the ratios of kinetic rate constants before and after mutation can be used to estimate the change in energy of the transition state (*31*, *33*). The ratio of the change in energy of the transition state over the ratio of the change in energy of the new equilibrium bound state (ϕ) is an indicator of how much of the mutated group's interaction is established by the transition state. If the toxin association and dissociation pathways pass through the same transition state, then $\phi_{on} = 1 - \phi_{off}$.

The ϕ_{on} for R13A and μ1 is 0.68, and the ϕ_{off} is 0.34. This result suggests that the Arg-13 interactions are not fully formed in the transition state and that the association and dissociation paths are similar (have the same rate-limiting step), because $1 - \phi_{off} \approx \phi_{on}$. Isolation of the extent of interaction of a particular pair of residues during the transition state can be made by performing mutant cycle analysis using the rate constants to reflect the change in energy. Then ϕ can be applied to particular pairs of residues. If ϕ_{on} is close to 0, then this interaction forms well after the transition state,

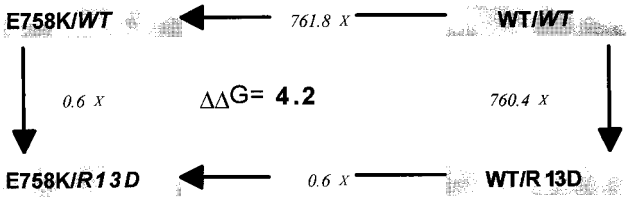

FIGURE 5: Example of mutant cycles. E758K/R13D produces a particularly large $\Delta\Delta G$ because of the improvement in binding produced by these complementary charge-reversing mutations. Energies ($\Delta\Delta G$) are in kilocalories per mole. The changes in binding affinity with each mutation are shown at the perimeter of each square. WT represents the wild-type μ1 channel. Script WT represents the wild-type μ-CTX.

and if ϕ_{on} is close to 1.0, the interaction forms well before the transition state. Intermediate values suggest that these interactions are partially formed at the transitional stage. Again, ϕ_{on} results should be complementary to ϕ_{off} results. This analysis suggested that Arg-13−Glu-403 and Arg-13−Tyr-401 interactions form significantly after transition. Asp-400 and Glu-758 were partially formed. The predictions from ϕ_{on} and ϕ_{off} for Lys-1237, Glu-755, and Asp-1532 were inconsistent, as if these groups formed new partners during the transition state.

Does R13 Block the Pore Directly? Several lines of evidence suggest an important role for Arg-13 in the block of current when μ-CTX is bound to Na^+ channels. When μ-CTX is bound, Arg-13 is clearly located in the outer vestibule, where it can interact closely with residues in the outer charged ring. Its closer interactions with Glu-758 and Glu-403 place μ-CTX closer to domains I and II, rather than being centered over the vestibule. Alterations in the Arg-13 substitution modulate the amount of current passed when the toxin is associated with the channel. All Arg-13 substitutions result in residual current when μ-CTX is bound to native μ1, and the residual current increases progressively when Arg-13 was substituted for lysine ($\leq$8%), glutamine and alanine (28 and 31%), and aspartate (56%). There are several ways whereby different substitutions at the Arg-13 position might modulate current, including (1) variable amounts of interaction between Na^+ and Arg-13 substitutions positioned in the outer vestibule, (2) variable coordination with channel residues necessary for conduction, (3) incremental conformational changes that alter pore size depending on the residue at the Arg-13 site, or (4) progressive modulation of the tightness of the μ-CTX fit within the outer vestibule as a function of the Arg-13−channel attraction. While the amount of Na^+ near the pore might be affected by Arg-13 substitutions in a manner that could explain the scaling of residual currents, the data suggesting that R13K allows some residual current implies that the presence of a

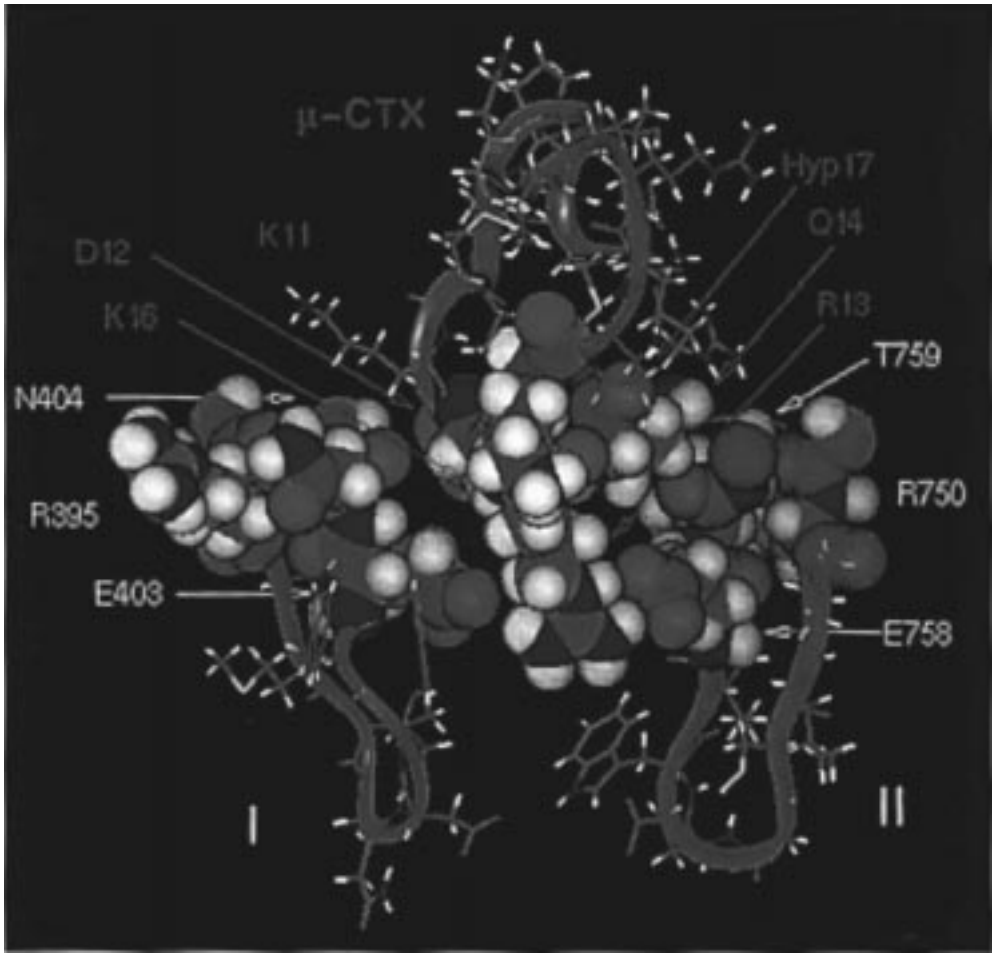

FIGURE 6: Molecular model of the μ-CTX−Na^+ channel interaction. Optimal arrangement of residues of the interactive surface of μ-CTX relative to the domains I and II outer vestibule rim. The μ-CTX backbone is in blue. Space-filling images for Asp-12, Arg-13, Gln-14, and Lys-16 are used for emphasis (carbon is green, nitrogen red, and hydrogen white). The vestibule backbone is in green, and residues Arg-395, Asp-404, Arg-750, and Thr-759 are highlighted. The toxin interactive surface is in van der Waals contact with the outer row of residues, and Arg-13 is close to Glu-758 and Glu-403.

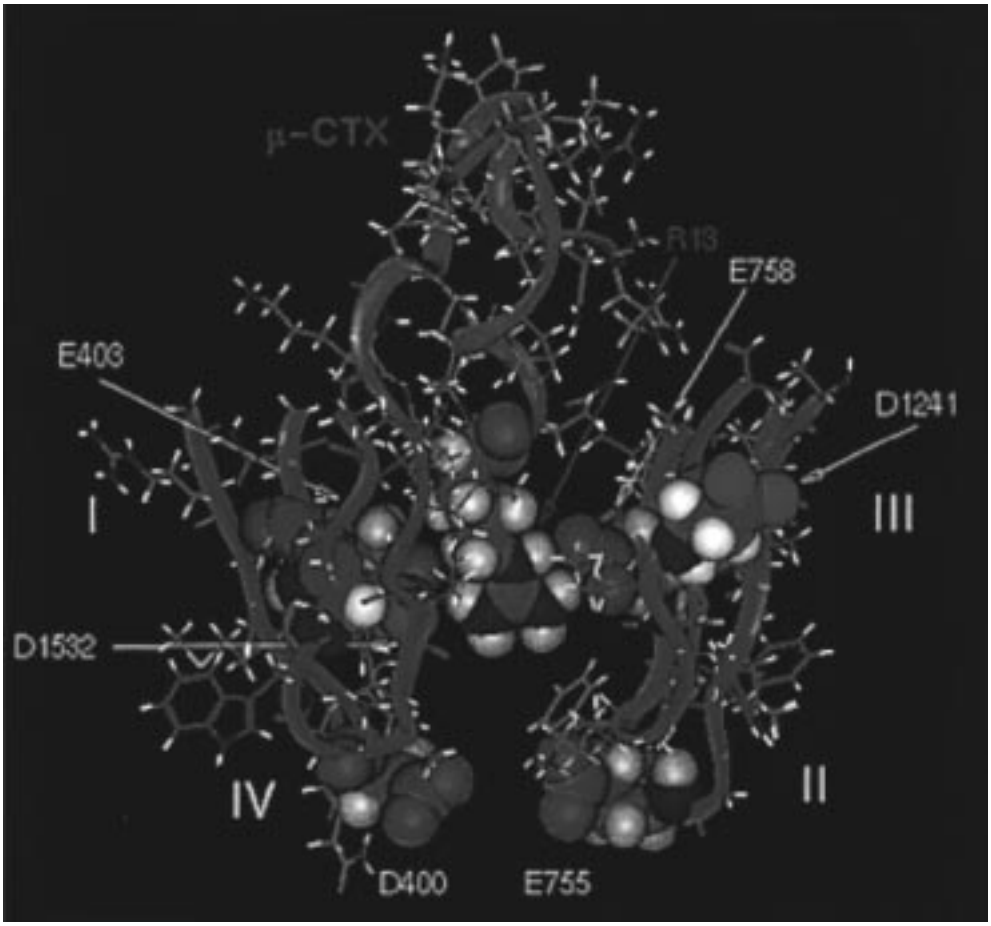

FIGURE 7: Spatial model of the complex of μ-CTX with respect to the P loops of all four domains. Arg-13 and critical carboxyl residues of the vestibule (including Glu-403, Glu-758, D-400, Glu-755, Asp-1241, and Asp-1532) are identified as space-filling elements. The projection is slightly rotated from that in Figure 6 to allow better visualization of the relation of Arg-13 to the vestibule residues.

toxin positive charge in the outer vestibule may be insufficient to cause complete current block. A definite choice as to mechanism is not possible on the basis of these experiments, but it seems likely that μ-CTX is eccentrically placed over the vestibule and under some conditions may allow a narrow pathway for ion permeation.

Illustration of Arg-13 Interaction in a Molecular Model of μ-CTX Docking. The experimental results reported here require that our previous proposal for the μ-CTX interaction with the Na^+ channel selectivity filter be modified (Figure 6). Although Arg-13 interacts with the vestibule, the toxin molecule does not reach deeply into the pore, probably because of its bulk. μ-CTX has high backbone structural rigidity (*20*), caused by its three disulfide bonds, and an egg-shaped spatial structure with Arg-13 at the bottom. The four residues nearest to Arg-13, which may be involved in the toxin interaction (Asp-12, Gln-14, Lys-16, and Hyp-17), are located approximately in a plane perpendicular to the side chain of Arg-13 and represent a candidate interactive surface with the outer vestibule rim. When μ-CTX was positioned into the vestibule so that the guanidinium group of Arg-13 was in immediate steric contact with the carboxyl group of Glu-758, as required by our experimental results, the nearby toxin residues were not in contact with the outer charged ring of the vestibule. That original vestibule model was constructed on the basis of TTX−STX interaction, and it was limited to eight amino acids from each domain (including Glu-403, Glu-758, and Asp-1532) because the small guanidinium toxins do not interact significantly with more distant residues (*2*, *6*−*8*).

To provide a channel interactive surface for the larger μ-CTX, the adjacent N-terminal and C-terminal residues were added to the original β-hairpins of each modeled domain to occupy the space between the original vestibule and the proposed toxin interactive surface (Arg-395, Asn-404, Arg-750, and Thr-759 for domains I and II). These residues are less well conserved (*40*) and are likely to be in external nonregular regions (*41*). Figures 6 and 7 show the proposed locations of these additional residues, extending the outer vestibule. Taking into account the predominant interaction of Arg-13 with domain I and II residues, energetic optimization yielded a preferred orientation of μ-CTX with respect to this putative outer rim, with immediate van der Waals contacts between the side chains of Lys-11, Asp-12, Gln-14, and Arg-1 residues and the main chain of channel residues of domains I and II. These external residues prevent the bulky μ-CTX from entering deeply into the pore. As a consequence, the guanidinium group of Arg-13 is in proximity to both carboxyl groups of Glu-758 and Glu-403, significantly above the putative selectivity filter residues (Asp-400, Glu-755, Lys-1237, and Ala-1529). This places the μ-CTX closer to domains I and II so that it only partially occludes the vestibule.

To determine if this structure conformed to our experimental results with Arg-13 and vestibule mutants, the interaction energies between pairs of residues in the model

were calculated with and without modeled mutations. The modeled interactions between Arg-13 and Asp-400 and Glu-755 were entirely electrostatic and between −1 and −1.5 kcal/mol, assuming complete ionization of the carboxyl residues. This is in agreement with the experimental results. Electrostatic interaction with Asp-1532 was smaller, barely reaching −1 kcal/mol, consistent with the data. Using the macroscopic dielectric constant measured by Dudley et al. (*19*) and Coulomb's law, these energies translate into distances of 9−10 Å. Similar distances can be estimated from the data of Schreiber and Fersht (*34*), who compared thermodynamic cycle analysis determination of interaction energies to spacing derived from the crystallographic structure of the barnase−barstar complex. The modeled interactions of Arg-13 with Glu-758 totaled −4.5 kcal/mol, with −3.0 kcal/mol representing the electrostatic energy and −1.5 kcal/mol representing the other nonbonded attractive energy. The nonbonded energy calculation agrees well with the experimental estimates, but the calculated electrostatic energy is somewhat greater than the experimental result. Possible reasons for this difference in estimates of the electrostatic energy include movement of the interacting residues after mutation to compensate for the loss of the Glu-758 interaction or incorrect p*K* values for the charged residues in the vestibule environment. Location of Arg-13 close to Glu-758 also places it close to Glu-403, resulting in a calculated electrostatic and nonbonded interaction with Glu-403 of −2 and −1.2 kcal/mol, respectively. The ΔG for the experimental mutation E403Q was almost −2 kcal/mol, as expected if the electrostatic interaction was lost, but the nonbonded interaction was maintained. It should be noted that arginine has a high frequency of salt bridge formation with multiple carboxyls between protein subunits or domains in structurally solved proteins (*42*), as was suggested by our measurements with Arg-13.

An interesting result of channel mutations on μ-CTX affinity has been reported by Li et al. (*39*). They found that the mutations W402C, W1239C, and W1531C enhanced μ-CTX affinity and suggested that these bulky tryptophans may interfere with optimal binding of μ-CTX. In our model of the vestibule, these tryptophan residues face outward, rather than into the vestibule, and do not interact directly with μ-CTX. Consequently, their side chains would not be expected to hinder μ-CTX interaction with the residues identified in our study. Cysteine is a particularly unusual substitute for tryptophan (*43*), and this mutation may have indirect effects such as enhancing the flexibility of the backbone and allowing interactions between μ-CTX and the adjacent glutamates to be optimized.

In summary, μ-CTX does not have a close association with the selectivity filter, in contrast to the proposed blocking complexes of TTX and STX (*1*, *44*). The close interaction with Glu-758 places μ-CTX in the vestibule mouth, where it interacts with channel residues in the Na^+ channel vestibule. The shape of the outer vestibule probably prevents Arg-13 from reaching the selectivity ring. Furthermore, the toxin appears to be eccentrically placed over the mouth of the vestibule, partially occluding it. An extended model of the outer vestibule is consistent with our results implying interactions of Arg-13 with vestibule charged residues, and it predicts testable interactions with the other residues of μ-CTX.

ACKNOWLEDGMENT

We thank Dr. Denis McMaster (Peptide Synthesis Core Facility, Department of Medical Biochemistry, University of Calgary, Calgary, Canada) for synthesis and purification of the μ-conotoxin derivatives. We thank Dr. Dorothy Hanck and Mr. Richard Benzinger for valuable discussions and Bei Li, Ian Glaaser, and Yu Huang for technical assistance.

REFERENCES

1. Lipkind, G. M., and Fozzard, H. A. (1994) *Biophys. J. 66*, 1−13.
2. Terlau, H., Heinemann, S. H., Stühmer, W., Pusch, M., Conti, F., Imoto, K., and Numa, S. (1991) *FEBS Lett. 293*, 93−96.
3. Heinemann, S. H., Terlau, H., Stühmer, W., Imoto, K., and Numa, S. (1992) *Nature 356*, 441−443.
4. Satin, J., Kyle, J. W., Chen, M., Bell, P., Cribbs, L. L., Fozzard, H. A., and Rogart, R. B. (1992) *Science 256*, 1202−1205.
5. Backx, P., Yue, D., Lawrence, J., Marban, E., and Tomaselli, G. (1992) *Science 257*, 248−251.
6. Kontis, K. J., and Goldin, A. L. (1993) *Mol. Pharmacol. 43*, 635−644.
7. Perez-Garcia, M. T., Chiamvimonvat, N., Marban, E., and Tomaselli, G. F. (1996) *Proc. Natl. Acad. Sci. U.S.A. 93*, 300−304.
8. Perez-Garcia, M. T., Chiamvimonvat, N., Ranjan, R., Balser, J. R., Tomaselli, G. F., and Marban, E. (1997) *Biophys. J. 72*, 989−996.
9. Favre, I., Moczydlowski, E., and Schild, L. (1996) *Biophys. J. 71*, 3110−3125.
10. Schlief, T., Schönherr, R., Imoto, K., and Heinemann, S. (1996) *Eur. Biophys. J. 25*, 75−91.
11. Chen, S. F., Hartmann, H. A., and Kirsch, G. E. (1997) *J. Membr. Biol. 155*, 11−25.
12. Tsushima, R. G., Li, R. A., and Backx, P. H. (1997) *J. Gen. Physiol. 109*, 463−475.
13. Moczydlowski, E., Olivera, B. M., Gray, W. R., and Strichartz, G. R. (1986) *Proc. Natl. Acad. Sci. U.S.A. 83*, 5321−5325.
14. Sato, K., Ishida, Y., Wakamatsu, K., Kato, R., Honda, H., Ohizumi, Y., Nakamura, H., Ohya, M., Lancelin, J. M., Kohda, D., and Inagaki, F. (1991) *J. Biol. Chem. 266*, 16989−16991.
15. Becker, S., Prusak-Sochaczewski, E., Zamponi, G., Beck-Sickinger, A. G., Gordon, R. D., and French, R. J. (1992) *Biochemistry 31*, 8229−8238.
16. Chen, L.-Q., Chahine, M., Kallen, R. G., Barchi, R. L., and Horn, R. (1992) *FEBS Lett. 309*, 253−257.
17. Stephan, M. M., Potts, J. F., and Agnew, W. S. (1994) *J. Membr. Biol. 137*, 1−8.
18. Chahine, M., Chen, L.-Q., Fotouhi, N., Walsky, R., Fry, D., Santarelli, V., Horn, R., and Kallen, R. G. (1995) *Recept. Channels 3*, 161−174.
19. Dudley, S. C., Jr., Todt, H., Lipkind, G., and Fozzard, H. A. (1995) *Biophys. J. 69*, 1657−1665.
20. Lancelin, J.-M., Kohda, D., Tate, S.-I., Yanagawa, Y., Abe, T., Satake, M., and Inagaki, F. (1991) *Biochemistry 30*, 6908−6916.
21. French, R. J., Prusak-Sochaczewski, E., Zamponi, G. W., Becker, S., Kularatna, A. S., and Horn, R. (1996) *Neuron 16*, 407−413.
22. Bowman, S., Tischfield, J. A., and Stambrook, P. J. (1990) *Technique 2*, 254−260.
23. Higuchi, R. (1990) in *PCR protocols: A guide to methods and applications* (Innis, M. A., Ed.) pp 177−183, Academic Press, New York.
24. Meienhofer, J., Waki, M., Heimer, E. P., Lambros, T. J., Makofske, R. C., and Chang, C.-D. (1979) *Int. J. Pept. Protein Res. 13*, 35−42.
25. Becker, S., Atherton, E., and Gordon, R. D. (1989) *Eur. J. Biochem. 185*, 79−84.

26. Becker, S., Liebe, R., and Gordon, R. D. (1990) *FEBS Lett. 272*, 152−154.
27. French, R. J., and Horn, R. (1997) in *From Ion Channels to Cell-to-cell Conversations* (Latorre, R., and Saez, J. C., Eds.) pp 67−89, Plenum Press, New York.
28. Hidalgo, P., and MacKinnon, R. (1995) *Science 268*, 307−310.
29. Chiamvimonvat, N., Perez-Garcia, M. T., Ranjan, R., Marban, E., and Tomaselli, G. F. (1996) *Neuron 16*, 1037−1047.
30. Carter, P. J., Winter, G., Wilkinson, A. J., and Fersht, A. R. (1984) *Cell 38*, 835−840.
31. Matouschek, A., Kellis, J., Serrano, L., and Fersht, A. R. (1989) *Nature 340*, 122−126.
32. Horovitz, A., and Fersht, A. R. (1990) *J. Mol. Biol. 214*, 613−617.
33. Fersht, A. R., Matouschek, A., and Serrano, L. (1992) *J. Mol. Biol. 224*, 771−782.
34. Schreiber, G., and Fersht, A. R. (1995) *J. Mol. Biol. 248*, 478−486.
35. Li, R. A., Tsushima, R. G., and Backx, P. H. (1997) *Biophys. J. 72*, A3.
36. Escobar, L., Root, M. J., and MacKinnon, R. (1993) *Biochemistry 32*, 6982−6987.
37. Faiman, G. A., and Horovitz, A. (1996) *Protein Eng. 9*, 315−316.
38. Fersht, A. R., Wilkinson, A. J., Carter, P., and Winter, G. (1985) *Biochemistry 24*, 5858−5861.
39. Li, R., Tsushima, R., Kallen, R. G., and Backx, P. H. (1997) *Biophys. J. 73*, 1874−1884.
40. Goldin, A. L. (1994) in *CRC Handbook of Receptors and Channels, Volume II. Ligand- and voltage-gated ion channels* (North, R. A., Ed.) pp 73−112, CRC Press, Boca Raton, FL.
41. Zvelebil, M. J., Barton, G. J., Taylor, W. R., and Sternberg, M. J. E. (1987) *J. Mol. Biol. 195*, 957−961.
42. Musafia, B., Buchner, V., and Arad, D. (1995) *J. Mol. Biol. 254*, 761−770.
43. Creighton, T. E. (1993) *Proteins: Structures and Molecular Properties*, 2nd ed., W. H. Freeman and Co., New York.
44. Hille, B. (1975) *Biophys. J. 15*, 615−619.

BI9724927